SANDIA REPORT

Truncated MultiGaussian Fields and Effective Conductance of Binary Media

S. A. McKenna, B. van Bloemen Waanders, J. Ray and Y. M. Marzouk
Sandia National Laboratories, NM
Sandia National Laboratories, CA and
Massachussetts Institute of Technology, MA

⊞ Sandia National Laboratories

Truncated MultiGaussian Fields and Effective Conductance of Binary Media

Sean A. McKenna, and Bart van Bloemen Waanders
Sandia National Laboratories, Albuquerque NM 87185

Jaideep Ray
Sandia National Laboratories, Livermore CA 94551

Youssef M. Marzouk
Massachusetts Institute of Technology, Cambridge, MA 02139
{samcken,bartv,jairay}@sandia.gov, ymarz@mit.edu

Abstract

Truncated Gaussian fields provide a flexible model for defining binary media with dispersed (as opposed to layered) inclusions. General properties of excursion sets on these truncated fields are coupled with a distance-based upscaling algorithm and approximations of point process theory to develop an estimation approach for effective conductivity in two-dimensions. Estimation of effective conductivity is derived directly from knowledge of the kernel size used to create the multiGaussian field, defined as the full-width at half maximum (FWHM), the truncation threshold and conductance values of the two modes. Therefore, instantiation of the multiGaussian field is not necessary for estimation of the effective conductance. The critical component of the effective medium approximation developed here is the mean distance between high conductivity inclusions. This mean distance is characterized as a function of the FWHM, the truncation threshold and the ratio of the two modal conductivities. Sensitivity of the resulting effective conductivity to this mean distance is examined for two levels of contrast in the two modal conductances and different FWHM sizes. Results demonstrate that the FWHM is a robust measure of mean travel distance in the background medium. The resulting effective conductivities are accurate when compared to numerical results and results obtained from effective media theory, distance-based upscaling and numerical simulation.

Acknowledgment

Contents

Figures

Truncated MultiGaussian Fields and Effective Conductance of Binary Media

1   Introduction

Determination of a single effective property value from an assemblage of materials is a long standing research problem in a number of scientific and engineering fields. Here we focus on development of an effective conductivity value from a mixture of two materials (binary media) with distinct conductances. A simple conceptualization of the binary medium as inclusions of a high/low conductivity material within a continuous matrix of material having the opposite conductivity serves for discussion here.

Effective properties of materials composed of mixtures of two component materials have been the subject of study for heat conduction, electrical conductivity, magnetic permeability, and electrical permittivity [1, 2, 3, 4, 5, 6, 7, 8, 9]. Hashin and Shtrikman [8] demonstrate the mathematically analogous nature of calculations for effective values of the conductance terms in these varied fields. An extensive amount of work for binary media has focused on defining the theoretical bounding values for the effective properties of the medium [10, 11, 4, 8].

The same approaches to effective media equations hold for calculation of effective permeability, or hydraulic conductivity, in steady-state flow through porous media. Binary models of conductivity are widely applied in subsurface flow through porous media particularly for representation of permeability patterns in fluvial deposits (e.g., [12, 6, 13, 14, 15]). Additionally, fractured media are often characterized using a binary permeability model where the fractures represent strongly anisotropic, high conductivity inclusions embedded within a matrix of low conductance. Fractured media can be represented as linear or planar conductive elements within a less conductive background using discrete fracture representations [16, 17] or as representation of fractured zones within continuum models [18, 19, 20].

Previous work on binary fields in the context of flow through porous media has emphasized development of expressions for the effective conductance of the field as a function of the proportion of the high/low, conductivity phase. Effective medium theories (EMT) for binary assemblages have focused on using the conductivities and proportion of the two materials to determine an effective conductivity value [9, 21, 5, 22]. Initial development of these theories used spherical inclusions and more recent work has incorporated additional information on the shapes of the inclusions [23, 24, 25, 1, 2, 26].

Thorough reviews of variations of the EMT-based approaches with comparison to other methods can be found in: [10] and [27]. EMT-based approaches assume non-interaction between inclusions and therefore do not utilize information on the connectivity or interac-

tion of either phase with other inclusions of the same phase. In testing against numerical results, EMT-based approaches work best when the inclusion fraction is less than 50 percent (see [6, 10]).

The effective conductivity formula developed by [27] incorporates information on connectivity of high conductivity inclusions through the average path length within the low conductivity material. This novel approach motivates exploration of various measures of connectivity and different techniques for estimating the mean length between inclusions. A model for these mean distances tied to the geometry of binary media resulting from truncation of multiGaussian (mG) fields is proposed herein and the behavior of this model is compared to previously developed expressions for effective media and numerical results.

A number of numerical techniques are available for simulation of binary random fields. Indicator geostatistical techniques [28] based on definition of the spatial variation through a variogram provide an efficient means of generating stochastic realizations of binary fields [29, 30, 31]. Alternatively, indicator simulation approaches can be based on transition probabilities between indicator classes [32, 33]. Typical applications of geostatistical simulation techniques are focused on generation of fields with more than two classes, multiple indicator simulation, but they can also be used for the generation of binary fields. Less common approaches for generating spatial binary fields include object-based and Boolean models [34], generation of periodic media [35, 7] and pluriGaussian and truncated mG fields [34, 36].

Development of excursion set theory applied to truncated mG fields over the past 15 years has been driven by developments in medical imaging and astrophysics [37, 38, 39]. In particular, calculation of the expected values of the total area, number of distinct excursions and the average excursion size over a threshold value can be calculated from definition of the mG field and knowledge of the threshold value ([40, 41]). Excursion set theory is applicable to truncation with a single threshold or multiple thresholds that produce multiphase fields (e.g.,[42]). Phillips and Wilson [43] proposed mean threshold crossing distances to estimate correlation lengths of permeability. However, in contrast to the wide application of mG random fields in hydrogeology, use of excursion sets from truncated fields for characterization and modeling of heterogeneous media in groundwater studies has been limited.

We parametrize a form of distance-based uspcaling using point-process theory and properties of truncated Gaussian fields to develop an expression for the effective conductance of binary media. This new expression, truncated Gaussian distance-based upscaling (TG-DBU) differs from the existing distance-based upscaling in that it does not require instantiation of the binary field. This is helpful if the model is to be fitted to data to estimate model parameters. Section 2 summarizes distance-based upscaling and the salient aspects of point-process theory and truncated mG fields. Section 3 combines these three elements into an expression for effective conductance for isotropic inclusions within a background matrix. In Section 4, this new expression is compared to distance-based upscaling using full knowledge of the binary field as well as an existing analytical solution and numerical solutions. Section 5 compares various distance measures and examines the behavior of the average distance between inclusions in the neighborhood of the percolation threshold.

2 Estimation of Effective Conductivity

Development of the TG-DBU procedure is motivated by the goal of estimating the effective conductance of a binary medium created from thresholding a Gaussian random field without instantiation of that field. The two modal permeabilities, $K1$ and $K2$, are considered known. Given the threshold at which the field is truncated, and size of the Gaussian kernel used to create the field as defined by the full-width at half-maximum (FWHM) parameter, the effective permeability is estimated.

2.1 Distance-Based Upscaling

The distance-based upscaling (DBU) approach developed by [27] utilizes an estimate of the mean flowpath length between inclusions within the background (matrix) material as a measure of phase connectivity. Through application of a phase-change theorem, the DBU approach applies to high or low conductivity inclusions within a matrix of the opposing material. The DBU approach [27] serves as the foundation for our estimation approach and is briefly outlined here.

The basis of DBU is conceptualization of each inclusion as a rectangular object of dimensions (B_x, B_y) centered within a larger rectangular block, having the same orientation, of dimensions (L_x, L_y). Fixed pressure boundary conditions on each end of the block and no-flow boundary conditions on the opposite sides create steady, one-dimensional flow along the x-direction. Knudby et al [27] identified an approximate linear relationship between the inverse of the effective conductivity of the block $(K_B)^{-1}$ and the relative shape of the inclusion $(B_x/L_x)(B_y/L_y)$ and used this relationship along with harmonic and arithmetic conductivity bounds to develop an expression for $(K_B)^{-1}$:

$$\frac{1}{K_B} = \left(\frac{1}{K_A} - \frac{1}{K_H} \right) \frac{R - p_1}{\frac{1}{p_1} - p_1} + \frac{1}{K_H} \tag{1}$$

where K_A and K_H are the arithmetic and harmonic mean conductivities, respectively, p_1 is the proportion of high permeability material and:

$$R = \frac{B_x/L_x}{B_y/L_y} = \frac{1}{p_1} \left(\frac{B_x}{L_x} \right)^2 \in \left[p_1, \frac{1}{p_1} \right] \tag{2}$$

The expression for $(K_B)^{-1}$ can also be cast as a weighted mean of K_A and K_H.

$$\frac{1}{K_B} = \rho \frac{1}{K_A} + (1 - \rho) \frac{1}{K_H} \tag{3}$$

where ρ is the relative inclusion shape, R, normalized by p_1:

$$\rho = \frac{R - p_1}{\frac{1}{p_1} - p_1} \in [0, 1] \qquad (4)$$

The distance-based component of the DBU method enters as a normalized average distance, D_{norm}, of the flow in the background medium within the block:

$$D_{norm} = \frac{B_x - L_x}{L_x} \qquad (5)$$

The normalized inclusion shape, ρ, can be restated using D_{norm}:

$$\rho = \frac{2D_{norm} - D_{norm}^2}{1 - p_1^2} \qquad (6)$$

Expansion of these relationships from a single inclusion within a single block to a field of inclusions requires calculation of average values across the field for the inclusion dimensions, $\overline{B}_x$, $\overline{B}_y$ and block dimensions, $\overline{L}_x$, $\overline{L}_y$. A key element of this development is determination of the average distances between inclusions along the direction of flow; $\overline{D} = \overline{L} - \overline{B}$. The block domain is conceptualized as a virtual permeameter centered on each inclusion within the field. $\overline{R}$ then represents the average relative inclusion shape and $\overline{D}_{norm}$ is the normalized average distance between inclusions along the direction of flow weighted by the area of each connecting inclusion.

In the DBU approach, the average distance, $\overline{D}$, is calculated as a weighted average using distances, D, and inclusion areas A as measured directly on the binary field:

$$\overline{D} = \frac{\sum_{j=1}^{n} \sum_{i=1}^{n} D_{i,j} A_i A_j}{\sum_{j=1}^{n} \sum_{i=1}^{n} A_i A_j} \qquad (7)$$

with the average block dimension in the direction of flow, x, calculated as:

$$\overline{B} = \frac{\sum_{j=1}^{n} B_{x,i} A_i}{\sum_{i=1}^{n} A_i} \qquad (8)$$

The normalized distance between inclusions is: $\overline{D}_{norm} = \overline{D}/\overline{L}$. Use of these spatial averages renders the block conductivity estimate, K_B, as an effective conductivity, K_{eff} for the domain.

A strong advantage of the DBU is the incorporation of the phase interchange theorem [3]. This theorem provides a relationship between K_{eff} of a field with low conductivity inclusions in a high conductivity matrix (low-in-high, $LinH$) and the generally easier-to-estimate K_{eff} of a complementary field of high conductivity inclusions in a low conductivity matrix (high-in-low, $HinL$). The fixed head and no-flow boundaries are rotated 90 degrees and applied to the complementary field. The fluxes, Q, through the two fields are related by:

$$Q_{LinH}Q_{HinL} = K_1 K_2 (\Delta H)^2 \tag{9}$$

where ΔH is the pressure drop across both fields from the prescribed boundary conditions. The product of the effective conductivities for each field is equal to the product of the two conductivities in the binary field:

$$K_{eff(HinL)}K_{eff(LinH)} = K_1 K_2 \tag{10}$$

A key advantage of the phase interchange theorem is that it enables the calculation of the $LinH$ case for any geometry for which the $HinL$ solution is available.

Knudby et al [27] demonstrate accurate estimation of K_{eff} for a range of simulated fields created with Poisson placement of ellipses or rectangles as well as those created with transition probability-based geostatistical simulation. Within these fields, the ratios of the two conductivities range from 100 to 10,000. The DBU results are also compared with several other effective value approaches.

2.2   Excursion Sets and Kernel Size

Calculation of K_{eff} with the DBU method requires both creation of the binary field and calculation of all inclusion sizes and distances between proximal inclusions. Image processing algorithms are available for these calculations; however, the computational expense of these algorithms is non-trivial. Here, we develop an approach for estimation of K_{eff} based on DBU that estimates the average inter-inclusion distance without explicit creation or processing of the binary field. This new approach relies on properties of truncated Gaussian fields to estimate the inclusion sizes and the mean distance between them and is designed to be computationally efficient.

The model for spatially correlated multiGaussian (mG) fields is based on a Gaussian kernel:

$$G(x,y) = \frac{1}{2\pi|\Sigma|^{1/2}} \exp\left(-\frac{1}{2}d\Sigma^{-1}d^T\right) \tag{11}$$

where d is the distance vector containing d_x and d_y that are distances from any location (x,y) back to the origin of the Gaussian function x_0, y_0 (here (0,0) for the standard normal

distribution). In this work, the covariance matrix, $\Sigma = \sigma^2 I$, (where I is the identity matrix) is diagonal for the specific case of the kernel being aligned with the grid axes. Convolution of an uncorrelated mG field with a Gaussian kernel creates a realization of a correlated random field. A discretized uncorrelated mG field (e.g., as described on a mesh) can be created by simply sampling the field values at the mesh points i.i.d. from a standard normal.

The spatial correlation of the mG field is defined by the FWHM of the Gaussian kernel used to create the Gaussian field. The FWHM parameter is commonly used as a spatial measure in image processing:

$$FWHM = \sigma\sqrt{8\ln(2)} \tag{12}$$

where σ is the standard deviation of the Gaussian kernel. Truncation of a Gaussian field at a threshold u defines the $u-level$ excursion set:

$$X_u = \left\{ x \in R^d : Y(x) \geq u \right\} \tag{13}$$

and the variogram, of the random set X_u can be calculated:

$$\gamma_u(h) = \frac{1}{\pi} \int_0^{\arcsin(\sqrt{\gamma(h)/2})} \exp\left(-\frac{u^2}{2}(1+\tan^2(t)) \right) dt \tag{14}$$

at lag spacings h. Variogram models that are linear at the origin (e.g., exponential, hyperbolic) cause the perimeter of X_u to be infinite (see [34], Section 16.1) and we restrict our work here to Gaussian kernel functions.

Three related properties of the truncated Gaussian field (following [40]) are:

N, the number of pixels above the truncation threshold, u,
m, the number of distinct regions (inclusions) above the threshold, and
n, the number of pixels in each region,

with expectation relationship $E[N] = E[m]E[n]$. For threshold value, u, the number of cells above that threshold, N, is provided by the Gaussian cdf and the size of the domain, S:

$$E[N] = S \int_u^\infty (2\pi)^{-1/2} e^{-z^2/2} dz \tag{15}$$

The Euler Characteristic, EC, in $D = 2$ represents the number of connected objects in the domain minus the total number of holes within those objects. Therefore EC goes to 0.0 at $u = 0$ and EC becomes negative when $u < 0.0$ as the truncated field represents a single

domain-spanning object containing a large number of holes. In 2D, the absolute value of *EC* is the number of distinct inclusions of either phase within the opposite phase and is used here to determine $E[m]$.

$$E[m] = |EC| = |(2\pi)^{-(D+1)/2} W^{-D} u^{D-1} e^{u^2/2}| \tag{16}$$

where W is an alternative measure of the spatial correlation of the mG field defined as a fraction of the FWHM:

$$W = FWHM / \sqrt{4\ln(2)} \tag{17}$$

For a given threshold, u, the average object area is found from the expectation relationship:

$$E[n] = E[N]/E[m] = E[N]/|EC| \tag{18}$$

Figure 1 compares a direct calculation of *EC* using the Matlab Image Processing toolbox [44] with estimates made using Equation 16 across a range of u values increasing from left to right. The corresponding binary fields are also shown for several representative threshold values.
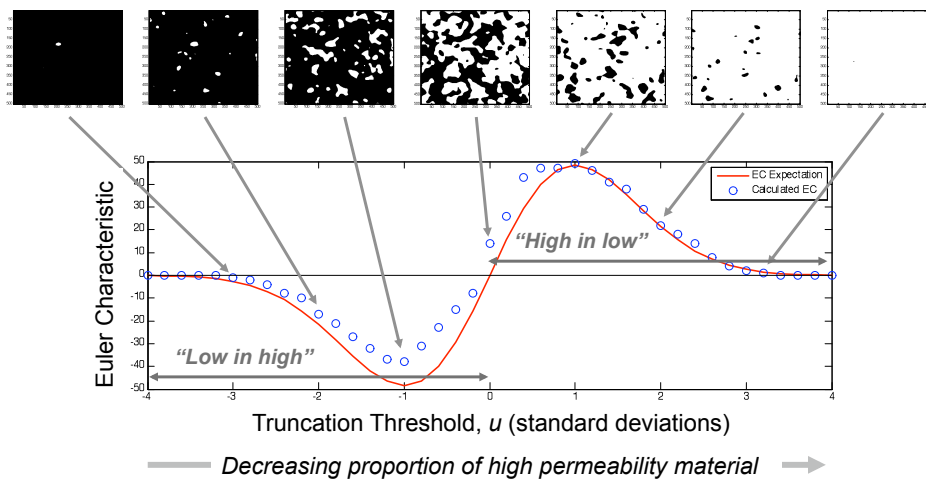

Figure 1. Calculated and estimated Euler characteristic for a truncated mG field as a function of u. The corresponding binary fields are shown for select thresholds. Regions of high conductivity are colored black.

13

This page intentionally left blank

3 Reduced Model Estimation

The properties of the truncated Gaussian field are used with the DBU method to develop an approximation for K_{eff} of a binary field. These estimations are done as a function of the proportion $[0, 1]$ of the high permeability phase (p_1) as defined by the threshold, u. A critical component of the DBU approach is $\overline{D}_{norm}$. We employ a combination of spatial point process theory and use of FWHM as a characteristic distance of the truncated field to estimate $\overline{D}_{norm}$ and refer to this approach as TG-DBU. The development here is for isotropic fields.

At u values near $-\infty$ or $+\infty$, the distances between centroids of inclusions are approximated as the distribution of nearest neighbor distances, d, from a Poisson point process (e.g., [45]) with an intensity $\lambda = |EC|/S$:

$$F(d) = 1.0 - \exp(-\pi \lambda d^2) : d \geq 0. \tag{19}$$

The estimated average distance between inclusion centroids, $\overline{D}^*$ is:

$$\overline{D}^* = \sqrt{\frac{S}{|EC|} \frac{1}{\pi}} \tag{20}$$

This approximation only holds at the extreme values of u (see [40]) as the distances between inclusion centroids overestimate the distance between inclusion edges as the average inclusion size, approximated as $E[n]$, increases. The value of $\overline{D}^*$ is adjusted to account for the inclusions having non-zero area by subtracting twice the average object radius $\overline{D}^* = \overline{D}^* - 2\sqrt{E[n]/\pi}$.

The DBU calculates distances between objects in the downstream direction only. The nearest neighbor distance calculation is adjusted to account for this preferential search direction through incorporation of a half angle, θ, that constrains the search for objects in the +/- 90 degree directions at $u = 0.0$ and with θ decreasing as u moves to the extreme values:

$$\theta = -2\pi(p_1 - 0.5)^2 + \pi/2 \tag{21}$$

This expression defines an exponential distribution for the variable θx^2 (after [45], page 34).

The geometry and connectivity of the binary patterns in truncated Gaussian fields vary considerably as u increases from $-\infty$ to $+\infty$ (Figure 1). Near the extreme values of u, the field is composed of independent high/low conductivity inclusions in a matrix of the opposite material. As u moves towards 0.0, the inclusions begin to coalesce forming larger inclusions with shapes that are roughly approximated by overlapping circles. At u values

even closer to 0.0, the inclusions begin to span the domain and at $u = 0.0$, there is no distinction between what is background and what is inclusion.

Conceptually, for the case of isotropic Gaussian fields the calculated value of $\overline{D}$ will never go to zero. As u moves towards 0.0 from either extreme, the $\overline{D}$ calculation changes from that of distances between isolated independent inclusions to distances between a few isolated inclusions and a main inclusion composed of several inclusions that were isolated at lower u values and finally to distances from one portion of a domain spanning inclusion across holes to another portion of that same inclusion.

At $u = 0.0$ ($p_1 = 0.50$) the average flow distance within the low permeability background should be equal to the FWHM distance. This assertion is due to the FWHM being the expected size of both the inclusions and the background matrix at this threshold.

This conceptualization provides the final piece of the effective conductivity approximation. For a given value of u, or the corresponding value of p_1, $\overline{D}$ is estimated as the larger of the average distance between inclusion edges and the *FWHM*:

$$\overline{D}^* = \max \left[\sqrt{\frac{S}{|EC|} \frac{1}{\pi}} - 2\sqrt{E(n)/\pi}, FWHM \right] \tag{22}$$

and used with Equation 1 to calculate K_B. This formulation is referred to as the *basic model* in the remainder of this paper. Figure 2 compares the results of the basic model against effective conductances calculated numerically using MODFLOW-2005, [46]. Harmonic averaging is used to calculate internodal conductances within MODFLOW. An ensemble of 30 mG fields are created on a 500×500 grid (with cells of unit size) with a convolution kernel of FWHM of 37.7 length-units. These mG fields are transformed to binary fields through truncation at thresholds corresponding to uniformly spaced changes in the proportion of the high conductivity phase from $p_1 = 0.04$ to 0.96. Additionally, thresholds of $u = $ -2.5 and 2.5 are used to create the minimum and maximum p_1 values for each field: 0.0062 and 0.9938. This process results in truncation of each field at 26 unique thresholds. For each of the 26 u threshold values, the average numerical result across 30 fields (780 evaluations) is shown. We define the ratio: $K1/K2$ using the log10 conductivity values: $\kappa = \log_{10}(K1) - \log_{10}(K2)$ and show results for $\kappa = 2$ and 4 in Figure 2.

The basic model utilizes an exceedingly simple parameterization of the mean distance between inclusions and produces relatively accurate estimates of the effective conductance. The basic model estimates are less than a factor of 2 (100 percent error) away from the numerical results for the case of $\kappa = 2$ for all values of p_1 with the most accurate results for $p_1 < 0.50$. The basic model tends to overestimate the numerical results at p_1 values greater than 0.50. For the case of $\kappa = 4$, the basic model strongly overestimates the numerical results at $p_1 > 0.50$.

Several extensions to the basic model distance calculations are incorporated for the final TG-DBU model. At low values of p_1, the basic model underestimates the numerical results
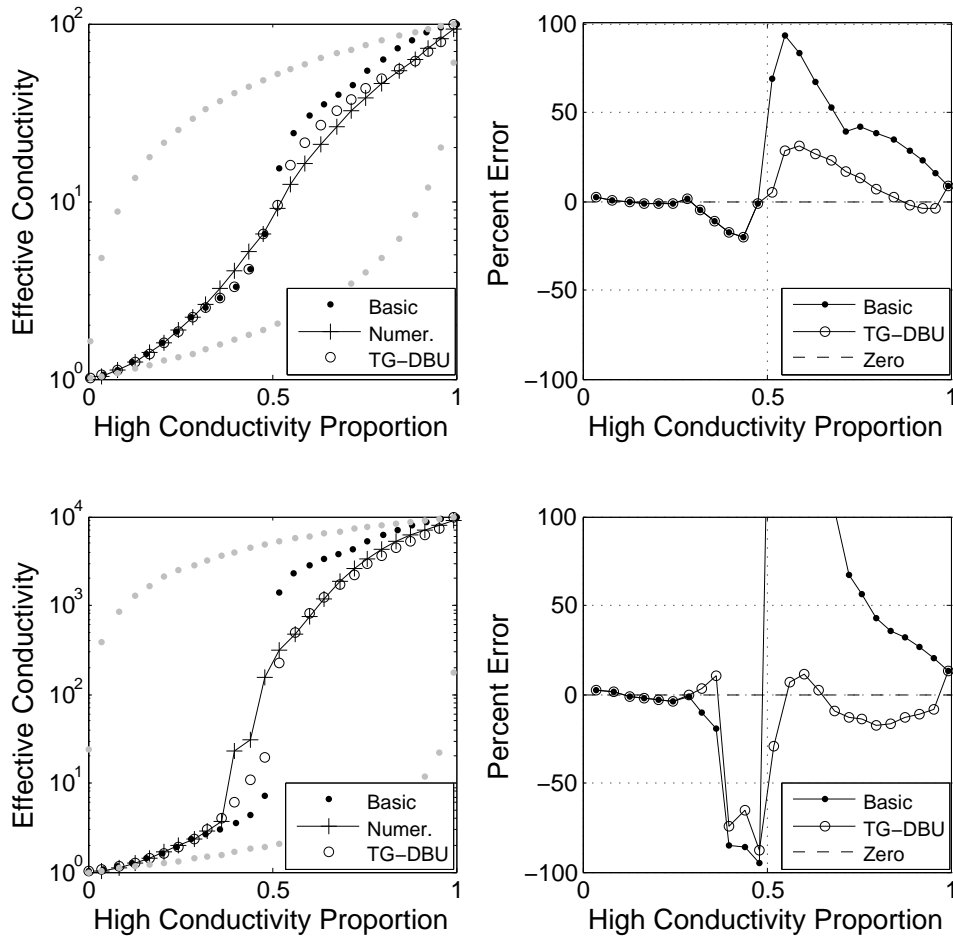
Figure 2. Comparison of effective conductivity values estimated with the basic model and the TG-DBU approaches to numerical results. The percent error of the effective conductivity solutions relative to the numerical results are shown in the right hand images. Results for two and four orders of magnitude difference in the modal conductivities are shown in the top and bottom rows, respectively. Results are for Gaussian fields created with an FWHM of 37.7 ($\sigma = 16.0$) length-units. The gray dots indicate the limiting values of the arithmetic and harmonic averages

and smaller distance values are needed to minimize this error. Additionally, the degree of underestimation increases with increasing κ (Figure 2). At levels of p_1 above 0.50, the basic model overestimates the numerical results and, due to application of the phase change theorem at these higher proportions, the distances must also be decreased in this region. The correction here must also be a function of κ.

The extended distance calculation is:

$$
\overline{D}^* = \begin{cases} \max\left[\sqrt{\frac{S}{|EC|}\frac{1}{\pi}} - 2\sqrt{E(n)/\pi}, \frac{FWHM}{(\kappa-1.0)} \right] & \text{for } p_1 < 0.50 \\[3em] \max\left[\sqrt{\frac{S}{|EC|}\frac{1}{\pi}} - 2\sqrt{E(n)/\pi}, FWHM \times (1.0-p_1)^{\kappa-1} \right] & \text{otherwise.} \end{cases}
$$

(23)

The extended distance calculations significantly improve the ability of the TG-DBU model to estimate the effective conductivity (Figure 2). For the case of $\kappa = 2$ the maximum error is reduced to less than 40 percent and for the $\kappa = 4$ case, the maximum error is less than 100 percent with the largest improvement occurring at p_1 values greater than 0.50.

4 Comparison to Analytical and Numerical Results

The TG-DBU estimated effective conductivity values are compared to existing models for values of p_1 in $[0, 1.0)$ and for κ values of 2 and 4. The harmonic and arithmetic means provide the upper and lower bounds on possible values. Visual comparisons and calculations of the percent relative error between the estimated values and numerical results are examined for two inclusion sizes. Comparisons are made to a self-consistent effective medium approximation developed by Pozdniakov and Tsang [25] that also employs the phase interchange theorem. Additionally, a series of binary fields are created from truncation of mG fields and used as input to the DBU approach of [27] as well as numerical calculation of effective conductivity.

Pozdniakov and Tsang [25] developed a self-consistent approach to the estimation of effective conductivity of binary media in 2D and 3D domains. The solution of [25] accounts for interaction between inclusions and uses the phase-interchange theorem to provide effective conductivity estimates across all proportions of high/low conductivity material. Equation 14 of [25] provides an analytic solution for the effective conductivity in a 2D domain with circular (isotropic) inclusions.

$$K_{eff} = (K_1 - K_2)(p_1 - 1/2) + 1/2\sqrt{(1 - 2p_1)^2(K_1 - K_2)^2 + 4K_1K_2} \tag{24}$$

The DBU approach of [27] as outlined in Section 2 is applied to each binary field. The same fields are also used as input to numerical calculations done with MODFLOW-2005 ([46]). For each inclusion size, DBU and numerical results are calculated on 30 fields at each of 26 thresholds.

Results comparing the model developed here to results of the self-consistent approach [25], the DBU approach [27] and numerical results are shown in Figure 3. These results were created from fields with a FWHM of 37.7 length-units. The TG-DBU and the self-consistent results ("PT 2004") are calculated independently of the actual binary field and require the phase proportions, the two modal conductances and the inclusion shape as inputs. The TG-DBU also utilizes the FWHM as an input. The DBU and numerical results are dependent on the actual binary fields, and for these results, each value in Figure 3 represents the average conductance calculated over 30 realizations. The deviations of the DBU estimates from the numerical estimates at proportions just above 0.50 appear to be an artifact of the distance calculations done here on the truncated mG fields and not a function of the DBU technique [27].

The right-hand side of Figure 3 shows the percent error of the three estimators relative to the numerical results. The axes are limited to +/- 100 percent, or a factor of +/- 2, for calculations where the modal conductivities vary by factors of 100 (top) and 10,000 (bottom). Relative to the self-consistent approach, the two distance-based upscaling techniques better capture the effective conductivity at proportions of the high conductance phase $p_1 > 0.50$.
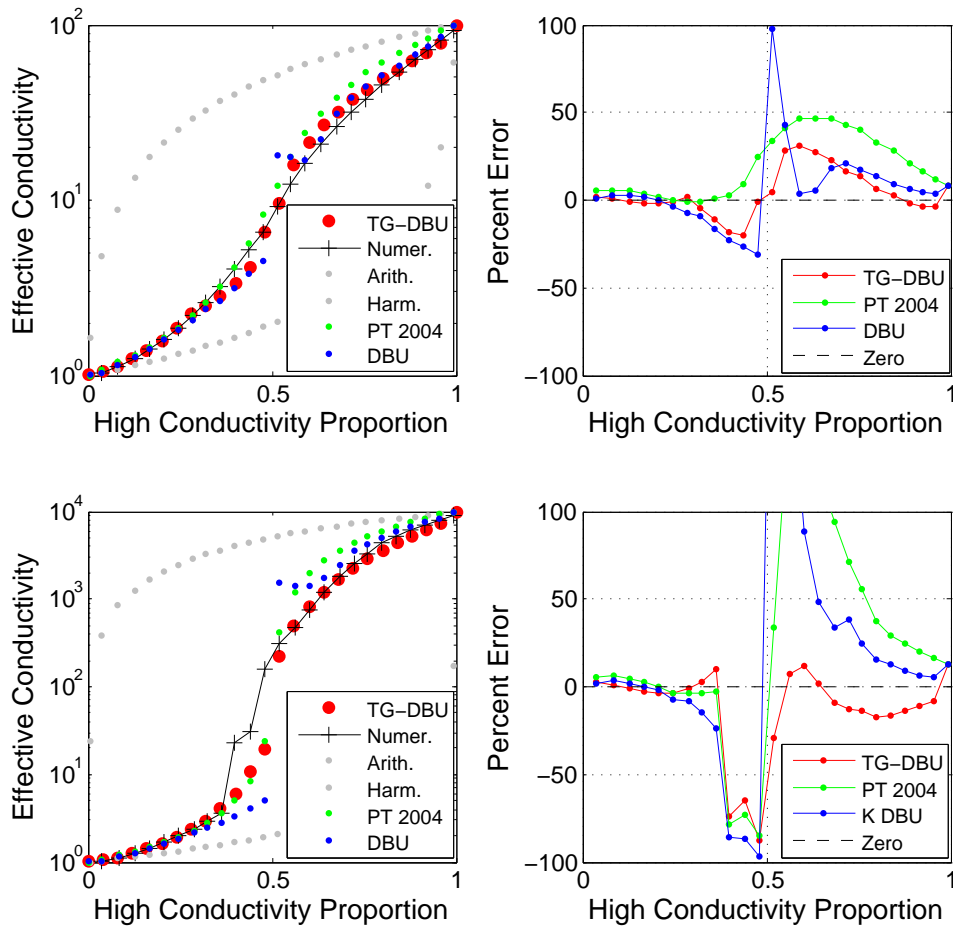
Figure 3. Comparison of estimated effective conductivity results, to the self-consistent solution, the DBU solution, the numerical results and the harmonic and arithmetic average bounds. The percent error of the effective conductivity solutions relative to the numerical results are shown in the right hand images. Results for two and four orders of magnitude difference in the modal conductivities are shown in the top and bottom rows, respectively. Results are for Gaussian fields created with an FWHM of 37.7 ($\sigma = 16.0$) length-units.

For all three approaches, errors are highest at or near $p_1 = 0.50$. This proportion corresponds to the bond percolation threshold for a square lattice in 2D [9] and represents the change point where the high conductivity phase becomes fully connected across the domain. Percolation theory and the percolation threshold have been developed for systems with no spatial correlation and are applied here where the ratio of FWHM to domain size is small (i.e., < 0.10). For these calculations, the size of the FWHM relative to the domain size is 0.075.

The approaches examined in this study define an effective conductivity for the domain. Effective properties are meaningful in cases where the domain size is much larger than the correlation length of the random field contained within the domain. This condition is also the definition of an ergodic field and a rule of thumb is that an effective property can be assigned to a domain when the correlation length is ≤ 0.10 of the domain size. In cases where the domain is discretized into smaller cells, or blocks, and the correlation length exceeds this limit relative to the cell size, a *block* property is assigned. Additional details on effective versus block properties are provided in [10].

As the FWHM increases, development of phase connection across the domain will occur at lower proportions of that phase. Figure 4 shows the results of calculations for a FWHM of 73.4 length-units, or 0.15 of the domain size.

The increase in the relative size of the inclusions decreases the proportion of high-conductivity material necessary to make a connected phase across the domain and the effective medium techniques tend to underestimate the numerical conductivity beginning at approximately p_1 $= 0.30$. This underestimation is particularly apparent in the $\kappa = 4$ results. All techniques examined are able to create reasonable estimates of the block conductivity at p_1 values > 0.6. These results provide motivation for future work to improve block conductivity estimates by incorporating percolation threshold behavior into the TG-DBU formulation.
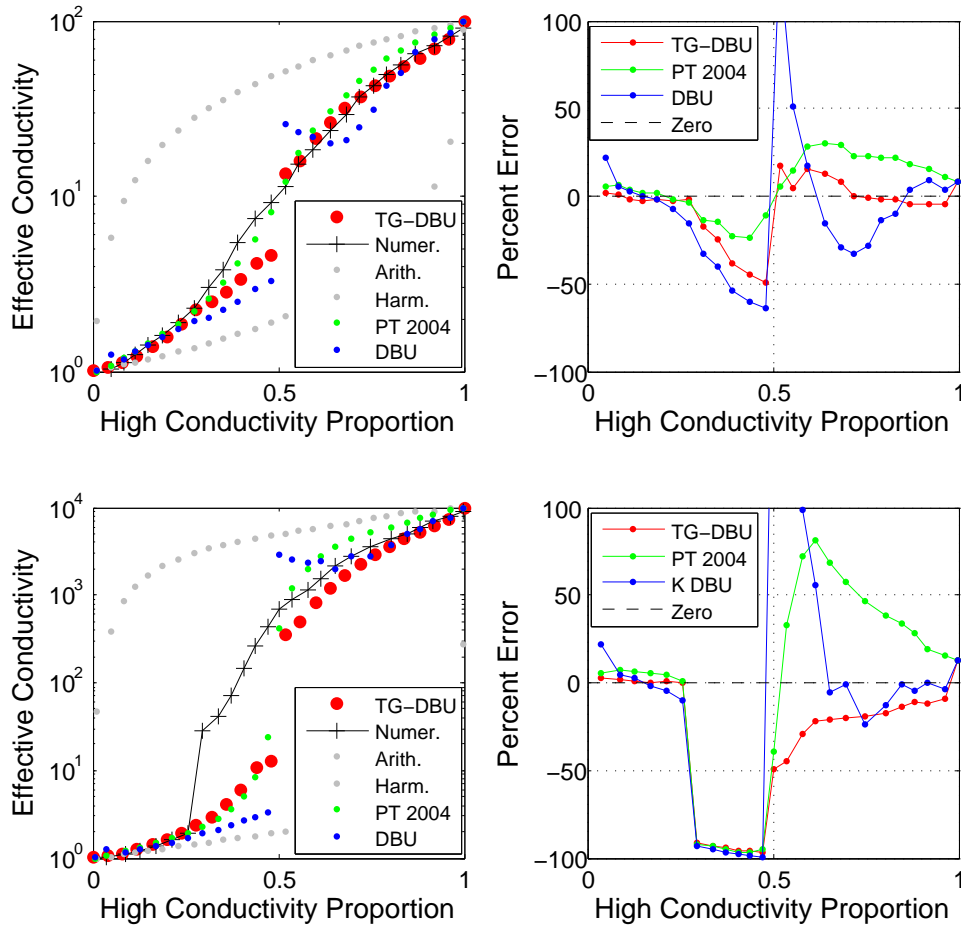
Figure 4. Comparison of estimated effective conductivity results, to the self-consistent solution, the DBU solution, the numerical results and the harmonic and arithmetic average bounds. The percent error of the effective conductivity solutions relative to the numerical results are shown in the right hand images. Results for two and four orders of magnitude difference in the modal conductivities are shown in the top and bottom rows, respectively. Results are for Gaussian fields created with an FWHM of 73.4 ($\sigma = 32.0$) length-units.

5   Results and Discussion

The value of $\overline{D}$ is a key feature of the the DBU and TG-DBU approaches and final effective conductances are sensitive to these values. Distance calculations are explored further in Figure 5 and compared to average distances across the background material as calculated along streamlines.

The basic model and the DBU model derive average distances from purely geometrical considerations and these values do not change as a function of κ (Figure 5). The average distances along streamlines are also quite stable across the change in κ while the TG-DBU approach explicitly incorporates the κ value into the average distance calculation. With the exception of the TG-DBU model, the FWHM serves as an excellent approximation of a lower limit on the distance values calculated by the different approaches.

The average distances from the streamline values are the largest of all calculated values. Examination of streamlines in truncated binary fields shows that streamline distances across the background material occurs where flow is nearly normal to the direction of the average gradient (Figure 6). This observation is counter to the development of the DBU and TG-DBU that limit the search across background material to other inclusions located in the downgradient direction. However, at p_1 values near 0.50 the FWHM is an excellent approximation of $\overline{D}$ both along the direction of the gradient and orthogonal to it. This observation of high local gradients creating flows in directions nearly normal to the average gradient is consistent with field observations and numerical model results for hydraulic gradient monitoring networks [47, 48].

The average distances calculated by the DBU method are weighted by the sizes of the inclusions on either end of the travel distance. In contrast, the TG-DBU employs a single average inclusion size, $E[n]$, thus weighting all distances equally. Figure 5 indicates that longer distances are generally connected to larger inclusions of high permeability material and are more highly weighted in the DBU approach. The distribution of distances calculated along streamlines are similarly skewed towards larger values.

The basic model and the DBU approach are developed as a function of p_1 and the average distances between objects. However, effective conductivity is not solely a function of the geometric arrangement of the inclusions. The κ value influences the average distance taken by flowpaths across the lower conductance material and simulations show that changes in κ have the largest impact on flow paths at p_1 values near 0.50. As an example, Figure 6 shows significant changes in the flow path locations for the same binary field at κ values of 2.0 and 4.0.

The average streamline distances are nearly unchanged from $\kappa = 2$ to $\kappa = 4$, yet Figure 6 shows significant changes in the locations of the streamlines on the same field for the two different κ values. The calculations of average distances for Figure 5 do not include a calculation at exactly $p_1 = 0.50$ (0.48 and 0.52 are the closest). The simulation results in Figure 6 are at exactly $p_1 = 0.50$ and show some difference with average streamline
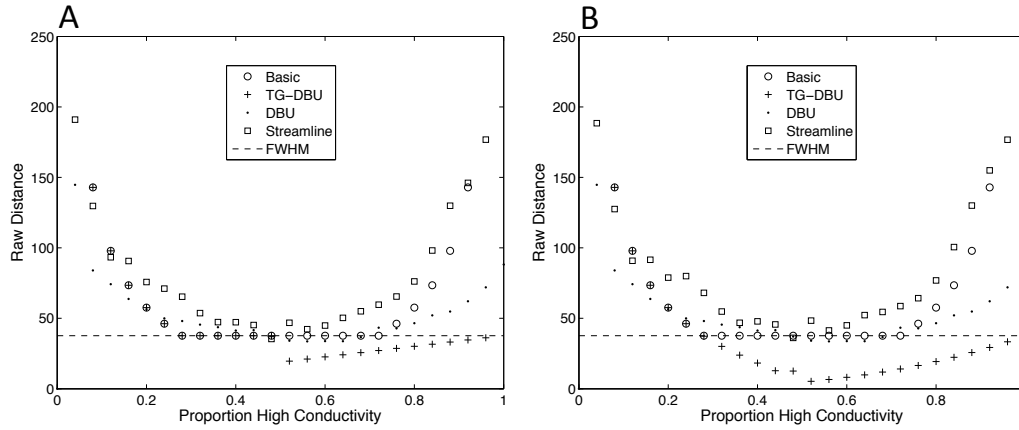
Figure 5. Comparison of average distance estimates for different calculation approaches. The DBU and Streamline results are average values calculated over 30 realizations. Results are for Gaussian fields created with κ values of 2 (A) and 4 (B) and an FWHM of 37.7 (σ = 16.0) length-units.

distances of 25.4 and 34.9 for the κ values of 2 and 4, respectively.

The impact of the κ value and the initiation of a percolating cluster may preclude application of distance-based uspcaling techniques for estimation of block-scale properties. Figure 7 shows both $\overline{D}$ calculated along streamlines and normalized by the FWHM and the effective conductance calculated numerically and normalized by the geometric mean conductance for four different truncated Gaussian fields. The region around $p_1 = 0.50$ is highlighted with flow and streamline solutions at p_1 increments of 0.008.

For each simulation with κ = 4, there is a significant increase in the effective conductance at the percolation threshold. This increase is not evident in the κ = 2 results. The average streamline distances between high permeability inclusions are not a strong function of p_1 and show gently decreasing values from $p_1 = 0.40$ to 0.60. These values are well approximated at p_1 values near 0.50 by the FWHM (ratio of 1.0) for both κ values. The vertical lines in Figure 7 indicate the location of the percolation threshold and vary from $p_1 <= 0.43$ to near 0.57 in these four example fields.

24
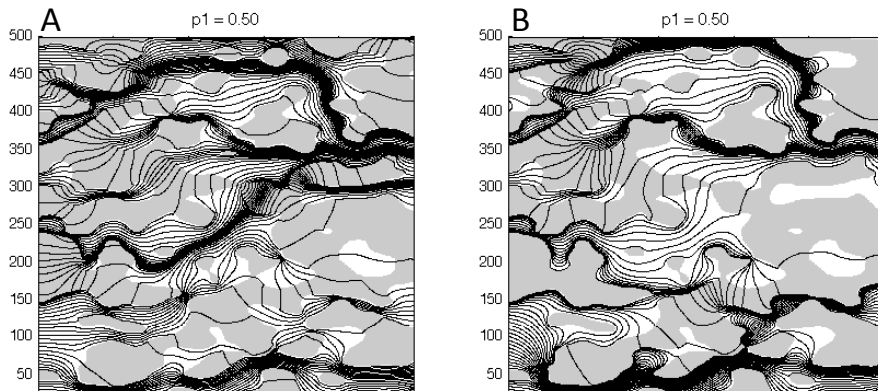
Figure 6. Comparison of flowpath locations for the same binary field with κ values of 2 (A) and 4 (B). Results are for Gaussian fields created with an FWHM of 37.7 (σ = 16.0) length-units and a threshold of u = 0.00 (p1 = 0.50). In both images, flow is from left to right.
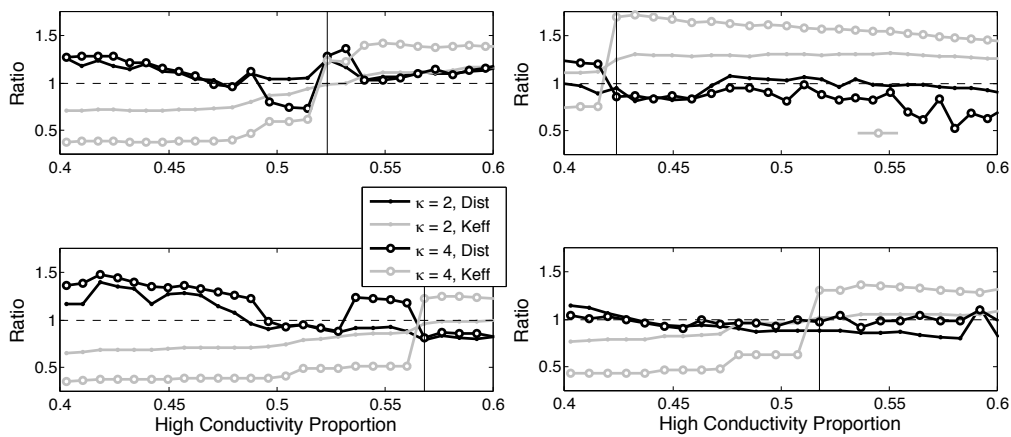
Figure 7. Effective conductances and average streamline lengths for p_1 values near 0.50. Results for four different fields are shown. The vertical black line denotes the percolation threshold. Effective conductances are normalized by the geometric mean conductance. Average streamline lengths are normalized by the FWHM.

This page intentionally left blank

6 Conclusions

This paper presents truncated mG fields as a flexible means of creating simulated binary media and then extends distance-based upscaling to directly utilize properties of the truncated mG fields to calculate effective conductivity values. Developments in medical image processing based on excursion set theory provide techniques for estimation of the number of inclusions, and average inclusion size from knowledge of the threshold and the kernel size (FWHM). These results are coupled with point process theory and distance-based upscaling (DBU) to develop a robust estimator of the effective conductivity of binary media. This new approach is called Truncated Gaussian-Distance Based Upscaling (TG-DBU). TG-DBU is based on expectation relationships and does not require instantiation of the binary field for estimation of the effective conductance.

TG-DBU is unique among upscaling approaches considered in that the kernel/inclusion size parameterized as the FWHM is a direct input to the upscaling function. We introduce the FWHM as a characteristic length for this upscaling and demonstrate its applicability for estimation of distances between inclusions across a broad range of p_1. Extensions to the geometrically-derived basic model that account for deviations in the estimated effective conductivities near the percolation threshold and account for the impact of κ on flow path distances between inclusions result in the TG-DBU model. Comparison of TG-DBU with numerical, DBU and self-consistent approaches demonstrates the accuracy of TG-DBU and shows results that are at least as accurate as the other techniques for all values of $p1$ for the fields examined.

Understanding the role of the average distance between inclusions and the sensitivity of this measure to other parameters is critical for further development of any distance-based upscaling techniques including TG-DBU. The impact of $p1$, κ and the percolation threshold on numerical calculations of effective conductivity and distances between inclusions along streamlines were examined. Results show that local gradients normal to the direction of the average gradient cause streamlines to traverse the background material in a direction orthogonal to the average flow direction. For isotropic media examined here, the FWHM value provides a robust approximation of the average streamline distance in the background material at $p1$ values near 0.50 and these results are not significantly impacted by percolation behavior or the value of κ. These results indicate that for anisotropic media where a maximum and minimum FWHM are used to define the Gaussian kernel, the FWHM normal to the flow direction will provide the best estimate of the average distance between inclusions. Effective conductances calculated across the percolation threshold indicate that the effective conductivity is a strong function of the κ value when $\kappa = 4$, but at $\kappa = 2$ the percolation threshold has little effect on the resulting effective conductance when the percolation threshold is reached. For the $\kappa = 2$ results, the geometric mean permeability serves as a reasonable estimate of K_{eff} on both sides of the percolation threshold. For the 30 fields examined, the percolation threshold is reached at p_1 values ranging from less than 0.40 to greater than 0.60 indicating that estimation of effective conductance values is possible, but that detailed knowledge of the field geometry and percolation threshold are necessary for

estimation of block-scale properties.

References

[1] T. Miloh and Y. Benveniste. A generalized self-consistent method for the effective conductivity of composites with ellipsoidal inclusions and cracked bodies. *Journal of Applied Physics*, 63(3):789–796, 1988.

[2] T. Miloh and Y. Benveniste. On the effective conductivity of composites with ellipsoidal inhomogeneities and highly conducting interfaces. *Proceedings of the Royal Society of London, A*, 455:2687–2706, 1999.

[3] K. Schulgasser. On the conductivity of fiber reinforced materials. *Journal of Mathematical Physics*, 17:382–387, 1976.

[4] G. W. Milton. Bounds on the electromagnetic, elastic and other properties of two-component composites. *Physical Review Letters*, 46(8):542–545, 1981.

[5] A. H. Sihvola and J. A. Kong. Effective permittivity of dielectric mixtures. *IEEE Transactions on Geosciences and Remote Sensing*, 26(4):420–429, 1988.

[6] A. J. Desbarats. Numerical estimation of effective permeability in sand-shale formations. *Water Resources Research*, 23(2):273–286, 1987.

[7] P. A. Fokker. General anisotropic effective medium theory for the effective permeability of heterogeneous reservoirs. *Transport in Porous Media*, 44(2):205–218, 2001.

[8] Z. Hashin and S. Shtrikman. A variational approach to the theory of effective magnetic permeability of multiphase materials. *Journal Applied Physics*, 33(10):3125–3131, 1962.

[9] M. Sahimi. *Flow and transport in porous media and fractured rock*. VCH, 1995.

[10] P. Renard and G. de Marsily. Calculating equivalent permeability: a review. *Advances in Water Resources*, 20(5-6):253–78, 1997.

[11] J. Rubinstein and S. Torquato. Flow in random porous media: mathematical formulation, variational principles and rigorous bounds. *Journal of Fluid Mechanics*, 206:25–46, 1989.

[12] H. H. Haldorsen and L. W. Lake. A new approach to shale management in field scale simulation models. *57th Annual Technical Conference, Society of Petroleum Engineers*, 1982.

[13] R. W. Ritzi, D. F. Jayne, A. J. Zahradnik, A. A. Field, and G. E. Fogg. Geostatistical modeling of heterogeneity in glaciofluvial, buried-valley aquifers. *Ground Water*, 32(4):666–674, 1994.

[14] R. W. Ritzi, D. F. Dominic, N. R. Brown, K. W. Kausch, P. J. McAlenney, and M. J. Basial. Hydrofacies distribution and correlation in the miami valley aquifer system. *Water Resources Research*, 31(12):3271–3281, 1995.

[15] G. E. Fogg. Groundwater flow and sand body interconnectedness in a thick, multiple-aquifer system. *Water Resources Research*, 22(5):679–694, 1986.

[16] J.-R. De Dreuzy, P. Davy, and O. Bour. Hydraulic properties of two-dimensional random fracture networks following a power-law length distribution: 1. effective connectivity. *Water Resources Research*, 37(8):2065–2078, 2001.

[17] L. Smith and F. W. Schwartz. An analysis on the influence of fracture geometry on mass transport in fractured media. *Water Resources Research*, 20(9):1241–1252, 1984.

[18] C. D. Langevin. Stochastic ground water flow simulation with a fracture zone continuum model. *Ground Water*, 41(5):587–601, 2003.

[19] S. A. McKenna and P. C. Reeves. Fractured continuum approach to stochastic permeability modeling. In T. C. Coburn, J. M. Yarus, and R. L. Chambers, editors, *Stochastic Modeling and Geostatistics: Principles, Methods and Case Studies, Volume II, AAPG Computer Applications in Geology 5*, pages 173–186. 2006.

[20] D. M. Reeves, D. A. Benson, and M. M. Meerschaert. Transport of conservative solutes in simulated fracture networks: 1. synthetic data generation. *Water Resources Research*, 44(W05404), 2008.

[21] K. S. Mendelsohn. A theorem on the effective conductivity of a two-dimensional heterogeneous medium. *Journal of Applied Physics*, 46(11):4740–4741, 1975.

[22] G. Dagan. Models of groundwater flow in statistically homogeneous porous formations. *Water Resources Research*, 15(1):47–63, 1979.

[23] G. Dagan. *Flow and transport in porous media*. Springer-Verlag, 1989.

[24] A. D. Poley. Effective permeability and dispersion in locally heterogeneous aquifers. *Water Resources Research*, 24(11):1921–1926, 1988.

[25] S. Pozdniakov and C. F. Tsang. A self-consistent approach for calculating the effective hydraulic conductivity of a binary, heterogeneous medium. *Water Resources Research*, 40, 2004. doi:10.1029/2003WR002617. W05105.

[26] R. W. Zimmerman. Effective conductivity of a two-dimensional medium containing elliptical inhomogeneities. *Proceedings of the Royal Society*, (452):A1713–A1727, 1996.

[27] C. Knudby, J. Carrera, J. D. Bumgardner, and G. E. Fogg. Binary upscaling: The role of connectivity and a new formula. *Advances in Water Resources*, 29:590–604, 2006.

[28] A. R. Solow. Mapping by simple indicator kriging. *Mathematical Geology*, 18(3):335–352, 1986.

[29] A. G. Journel and F. Alaber. Non-Gaussian data expansion in the earth sciences. *Terra Nova*, 1(2):123–134, 1989.

[30] J. J. Gomez-Hernandez and R. M. Srivastava. ISIM3D: An ANSI-C three-dimensional multiple indicator conditional simulation program. *Computers and Geosciences*, 16(4):395–440, 1990.

[31] *GSLIB: Geostatistical Software Library and User's Guide*. Oxford University Press, 1998.

[32] S. F. Carle and G. E. Fogg. Transition probability-based indicator geostatistics. *Mathematical Geology*, 28(4):453–476, 1996.

[33] S. F. Carle and G. E. Fogg. Modeling spatial variability with one and multidimensional continuous lag markov chains. *Mathematical Geology*, 29(7):891–918, 1997.

[34] C. Lantuejoul. *Geostatistical Simulation: Models and Algorithms*. Springer-Verlag, 2002.

[35] T. Harter and C. Knudby. Effective conductivity of periodic media with cuboid inclusions. *Advances in Water Resources*, 27(10):1017–1032, 2004.

[36] M. Armstrong, A. G. Galli, H. Beucher, G. Loch, D. Renard, B. Doligez, R. Eschard, and F. Geffroy. *Plurigaussian Simulations in Geosciences*. Springer, 2003.

[37] R. J Adler. On excursion sets, tube formulas and maxima of random fields. *Annals of Applied Probability*, 10(1):1–74, 2000.

[38] R. J. Adler, J. E. Taylor, and K. J. Worsley. *Applications of Random Fields and Geometry: Foundations and Case Studies*. 2009.

[39] J. E. Taylor and R. J. Adler. Euler characteristics for Gaussian fields on manifolds. *The Annals of Probability*, 31(2):533–563, 2003.

[40] K. J. Friston, K. J. Worsley, R. S. J. Frackowiak, J. C. Mazziotta, and A. C. Evan. Assessing the significance of focal activations using their spatial extent. *Human Brain Mapping*, 1:210–220, 1994.

[41] K. J. Worsley, S. Marrett, P. Neelan, and A. C. Evans. Searching scale space for activation in pet images. *Human Brain Mapping*, 4(1):74–90, 1996.

[42] D. J. Nott and R. J. Wilson. Multi-phase image modelling with excursion sets. *Signal Processing*, 80:125–139, 2000.

[43] F. M. Phillips and J. L. Wilson. An approach to estimating hydraulic conductivity spatial correlation scales using geological characteristics. *Water Resources Research*, 25(1):141–143, 1989.

[44] *Matlab, 2009a, Image Processing Toolbox*. Natick, MA, USA.

[45] P. J. Diggle. *Statistical analysis of spatial point patterns, Second edition*. Oxford University Press, 2003.

[46] A. W. Harbaugh. MODFLOW-2005, the U.S.Geological Survey modular ground-water model – the ground water flow process. U.S. Geological Survey Techniques and Methods 6-A16, U.S. Geological Survey, 2005.

[47] S. E. Silliman and C. Frost. Monitoring hydraulic gradients using three-point estimators. *Journal of Environmental Engineering*, 124(6):517–523, 1998.

[48] S. A. McKenna and A. Wahi. Local hydraulic gradient estimator analysis of long-term monitoring networks. *Ground Water*, pages 723–731, 2006.

DISTRIBUTION: